

Sub-system fault tolerance with the Bacon-Shor code

Panos Aliferis¹ and Andrew W. Cross^{2,3}

¹ Institute for Quantum Information, California Institute of Technology, Pasadena, CA 91125

² Massachusetts Institute of Technology, 77 Massachusetts Avenue, Cambridge, MA 02139

³ IBM Research Division, T. J. Watson Research Center, P. O. Box 218, Yorktown Heights, NY 10598
(Dated: May 25, 2019)

Sub-system encodings provide the most general way for protecting quantum information; however, their benefits for fault-tolerant quantum computation over standard sub-space encodings have not been explored so far. We show how the gauge freedom in the Bacon-Shor sub-system code [D. Bacon, Phys. Rev. A 73, 012340 (2006)] can be used to obtain remarkably simple and efficient procedures for fault-tolerant error correction (FTEC). Most notably, FTEC does not require entangled ancillary states and can be implemented using nearest-neighbor two-qubit measurements. Our lower bound on the quantum accuracy threshold, $1.94 \cdot 10^{-4}$ for adversarial stochastic noise, improves previous rigorous lower bounds by nearly an order of magnitude.

PACS numbers: 03.67.Pp

Operating a full-scale quantum computer will require methods for protecting against decoherence or systematic hardware imperfections; this is the realm of quantum fault tolerance. The cornerstone result in the theory of fault-tolerant quantum computation [1], the threshold theorem, maintains that any quantum computation can be efficiently simulated to any desired accuracy provided the noise strength (probability or amplitude, depending on the error model) of each elementary quantum operation is below a certain critical value, the quantum accuracy threshold [2]. Establishing better lower bounds on the value of the accuracy threshold and reducing the overhead for quantum fault tolerance are two of the main directions of current research on quantum computation. This paper presents improvements in both these fronts.

Protection of quantum information against noise is achieved by mapping the system to be encoded (e.g., one logical qubit) into a sub-system of a larger system [3]. Such a mapping provides the most general possible encoding once we require that the evolution and measurement statistics are identical for the encoded system and the encoding sub-system [4]. Letting H_S be the Hilbert space of the system to be encoded, the coding map identifies density operators and observables in H_S with density states and observables in a sub-system H_L of a larger Hilbert space H , $H = (H_L \otimes H_T) \otimes H_R$, where H_T describes additional sub-systems not necessarily protected by noise and H_R labels the "rest" of H . Standard sub-space encodings can be seen as sub-system encodings where H_T is one-dimensional encoding no sub-system. Conversely, for any sub-system encoding there exists a corresponding sub-space encoding obtained by projecting the state in H_T onto a pure state [5].

Because of this connection, sub-system encodings do not lead to quantum codes with fundamentally new properties beyond sub-space codes. Nevertheless, the error-correction procedures can differ substantially in the two cases. This is of interest for fault-tolerant quantum com-

putation, where the complexity of fault-tolerant error correction (FTEC) is an important determining factor for both the accuracy threshold and the overhead.

We will consider fault-tolerant quantum circuits where computation is encoded using a sub-system code due to Bacon [6]. Because of the close relation of this code with Shor's code [7], we will refer to it as the Bacon-Shor code. The Bacon-Shor code is a stabilizer CSS code encoding one logical qubit into a code block of n^2 physical qubits for some integer $n > 1$; in standard notation it is a $[[n^2; 1; n]]$ code, so its distance is n . Since Bacon's code construction really generates a family of quantum codes parameterized by the integer n , we will use the notation $C_{BS}^{(n)}$ for the distance- n member of this family.

It is convenient to place the n^2 qubits in the $C_{BS}^{(n)}$ block on the vertices of a $n \times n$ square lattice as shown in Fig. 1. Then, the code can be defined in terms of its stabilizer group [8]

$$S(C_{BS}^{(n)}) = \{ X_{\text{row } i; \text{row } (i+1)} ; Z_{\text{col } j; \text{col } (j+1)} \}_{i,j=1}^{n-1} \quad (1)$$

where we have used the short-hand notation for the Pauli matrices X and Z , $X_{\text{row } i; \text{row } (i+1)}$ denotes a tensor product of X operators acting on all qubits in rows i and $i+1$ and, similarly, $Z_{\text{col } j; \text{col } (j+1)}$ denotes a tensor product of Z operators acting on all qubit in columns j and $j+1$.

The code syndrome e , defined as the vector of eigenvalues of the $2(n-1)$ stabilizer generators in Eq. (1), induces a decomposition of the Hilbert space H of the n^2 qubits in the code block into sub-spaces encoding $n^2 - 2(n-1) = (n-1)^2 + 1$ logical qubits. Therefore, within each sub-space with fixed syndrome e and, in particular, within the code space corresponding to the trivial, all-zero syndrome $e=0$ we can define a sub-system decomposition

$$M = \{ H_L \otimes H_T \}_{e \in \text{eigen}(S(C_{BS}^{(n)}))} \quad (2)$$

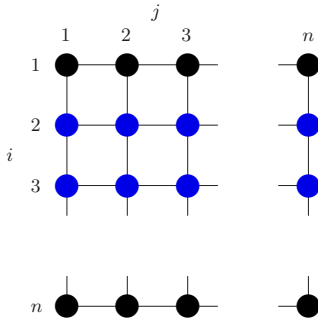


FIG. 1: (color online) Qubits in the $C_{BS}^{(n)}$ block are placed on the vertices of a $n \times n$ square lattice. One element of the code stabilizer is shown: $X_{\text{row } 2, \text{row } 3}$ applies X on all qubits shown in blue.

where we associate H_L with the one logical qubit protected by the full distance n of the code. The logical Pauli operators for this "protected" logical qubit are $X_L = X_{\text{row } 1}$ (i.e., a tensor product of X operators applied on all qubits in the first row) and $Z_L = Z_{\text{col } 1}$ (i.e., a tensor product of Z operators applied on all qubits in the first column). H_T we associate with the remaining $(n-1)^2$ logical qubits whose logical operators can be chosen from the non-abelian group

$$T = h X_{j;i} X_{j+1;i} ; Z_{i;j} Z_{i;j+1} ; j \in \mathbb{Z}_{n-1} ; i ; \quad (3)$$

where we have used the notation $O_{i;j}$ for an operator O acting on the qubit with coordinates $(i;j)$. Indeed, the operators in T commute with the stabilizer generators in Eq. (1), commute with the logical operators X_L and Z_L and, furthermore, can be grouped into $(n-1)^2$ independent pairs of anti-commuting operators, with operators in different pairs commuting.

Given some non-trivial syndrome value, error recovery proceeds in a similar manner as in the classical repetition code: The eigenvalues of the stabilizer generators $X_{\text{row } i, \text{row } (i+1)}$, for $i \in \mathbb{Z}_{n-1}$, can be used to correct Z errors on up to $b_0 = 2c$ rows. Moreover, only the parity of Z errors in each row is relevant: an operator acting as Z on a pair of qubits at the same row is an operator in T and, therefore, has no effect on the protected information in H_L . Error recovery for X errors proceeds similarly along the columns. Further intuition on the Bacon-Shor code can be obtained by considering its derivation from known sub-space codes; see Section A in the Appendix.

Since logical operators in H_T have weight two (i.e., act non-trivially on two qubits in the code block), if we take into consideration all $(n-1)^2 + 1$ logical qubits, then $C_{BS}^{(n)}$ is a distance-2 code. It is therefore error detecting but not, in general, error correcting. However, if we only consider the logical qubit encoded in H_L , then we effectively obtain a distance- n code and errors with support on up to $b_0 = 2c$ qubits can be corrected. In fact, error correction with respect to H_L will unavoidably result in non-trivial

logical operations being performed at the same time on H_T . This is not a problem as long as we never encode useful information in H_T . We can think of the $(n-1)^2$ logical qubits in H_T as "gauge" qubits as they correspond to degrees of freedom for the logical information encoded in H_L . In some cases it will be sufficient to disregard them. More interestingly, we will next discuss how we can design error-correction procedures that extract the code syndrome by manipulating the state of the gauge qubits.

To show how the gauge qubits can be used to our advantage, we first note that, $8j \in \mathbb{Z}_{n-1}$, we can write

$$\begin{aligned} X_{\text{row } j, \text{row } (j+1)} &= \prod_{i=1}^{n-1} (X_{j;i} X_{j+1;i}) ; \\ Z_{\text{col } j, \text{col } (j+1)} &= \prod_{i=1}^{n-1} (Z_{i;j} Z_{i;j+1}) ; \end{aligned} \quad (4)$$

What is remarkable about this decomposition is that the operators in parentheses act only on H_T as logical operators of the gauge qubits; hence, they commute with all stabilizer generators and also commute with the logical operators for the protected logical qubit in H_L . Because of this, we can measure each of them separately and then Eq. (4) implies that the code syndrome can be computed by taking the appropriate parities of the measurement outcomes. Moreover, since all of these operators act non-trivially only on two qubits in the code block, measuring each one of them is an especially easy task. For example, Fig. 2 shows simple circuits for measuring $X_{j;i} X_{j+1;i}$ or $Z_{i;j} Z_{i;j+1}$ using one ancillary qubit.

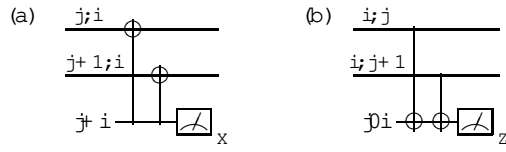


FIG. 2: (a) A circuit for measuring the operator $X_{j;i} X_{j+1;i}$ using one ancillary qubit. (b) A similar circuit for measuring $Z_{i;j} Z_{i;j+1}$.

This indirect method for inferring the syndrome by measuring two-qubit operators significantly reduces the overhead for FTEC. This is because, unlike in standard FTEC methods [2], this method does not require preparing and verifying entangled ancillary states: ancillary qubits in the $|j;i\rangle$ or $|j+1;i\rangle$ state are sufficient as in Fig. 2. Furthermore, for maximum qubit efficiency, a single ancilla can be used to sequentially measure all two-qubit operators necessary to extract the syndrome. The specific two-qubit operators to be measured can be chosen to have support on neighboring physical qubits when qubits in the code block are arranged on a two-dimensional lattice. For this reason, this FTEC method is especially advantageous for geometrically local architectures as those envisioned for ion-trap or solid-state implementations. Section B in the Appendix gives more details on this method and discusses its application to a two-dimensional setting.

In settings without geometric locality constraints or when qubit movement has error rate much lower than gates, other standard FTEC methods will yield the best accuracy thresholds. Since $C_{BS}^{(n)}$ is a CSS code, Steane's FTEC method (SteFTEC) [9] can be used to extract the syndrome provided we can fault-tolerantly prepare logical $\lvert \text{ji} \rangle$ ($\lvert \text{ji}_L \rangle$) and logical $\lvert \text{ji} \rangle$ ($\lvert \text{ji}_L \rangle$) states. Alternatively, Knill's FTEC method (KnifTEC) [10] requires fault-tolerantly preparing logical Bell states.

As is evident from the decomposition in Eq. (2), the distinctive feature of sub-system encodings is that logical states in H_L are not uniquely encoded: after having specified a logical state in H_L , the state in H_T can still be arbitrary. This freedom in choosing the state that is encoded in H_T can be used to our advantage in the design of encoding circuits for logical states in H_L . In particular, we will next discuss how, by exploiting this freedom, we can design remarkably simple encoding circuits for the logical ancillary states required for SteFTEC and KnifTEC, thus also reducing the complexity of post-encoding ancilla verification.

For concreteness, consider designing an encoding circuit for the logical $\lvert \text{ji} \rangle$ state; i.e., a state in the code space which is the $+1$ eigenstate of Z_L . With the logical state in H_L specified, we can choose the state in H_T to be the logical $\lvert \text{ji} \rangle$ for all gauge qubits, i.e., the $+1$ eigenstate of the gauge-qubit operators $X_{i;j} X_{i+1;j} Z_T, 8i, j$. In other words, our encoding circuit encodes the logical $\lvert \text{ji} \rangle$ state in H_L by preparing a $+1$ eigenstate of the operators in the following stabilizer group:

$$S(\lvert \text{ji}_L \rangle) = hX_{i;j} X_{i+1;j} Z_{\text{col } j} \lvert \text{ji} \rangle Z_{n-1} \lvert \text{ji} \rangle Z_n \lvert \text{ji} \rangle. \quad (5)$$

We recognize the state described by Eq. (5) as a tensor product of n Schrödinger "cat" states in the Hadamard-rotated basis, each one lying across a column n in Fig. 1.

We can obtain the logical $\lvert \text{ji} \rangle$ state by applying a logical Hadamard transformation to the logical $\lvert \text{ji} \rangle$ state. We observe that applying transversal Hadamard gates has the same effect on the encoded information as a logical Hadamard gate up to a 90-degree rotation of the square lattice in Fig. 1. We can therefore obtain $\lvert \text{ji} \rangle$ by first preparing $\lvert \text{ji}_L \rangle$, applying transversal Hadamard gates and, finally, physically rotating the lattice in Fig. 1 by 90 degrees. The transversal Hadamard gates will transform the Hadamard-rotated cat states to become usual cat states in the computation basis. And then, rotating the lattice by 90 degrees will align the n cat states each to lie across a row – this is our construction for $\lvert \text{ji}_L \rangle$. Having designed the encoding circuits for both $\lvert \text{ji}_L \rangle$ and $\lvert \text{ji}_L \rangle$, logical Bell states to be used in KnifTEC can be constructed by interacting these two logical states via a logical CNOT gate (as for all CSS codes, the logical CNOT gate for $C_{BS}^{(n)}$ is transversal). Section C in the Appendix gives further details on SteFTEC and KnifTEC and Section E presents explicit FTEC circuits using these two methods.

As we have already discussed, the logical CNOT and Hadamard gates are transversal for the Bacon-Shor code. Universal quantum computation can be realized by including the logical phase gate $S = \exp(-i\frac{\pi}{4}z)$ and the logical Toffoli gate in our gate set. The details of achieving encoded quantum universality with the Bacon-Shor code are discussed in Section D in the Appendix.

We have analysed the accuracy of fault-tolerant circuit simulations using the concatenated $C_{BS}^{(n)}$ for various values of n . In our analysis, we have considered two error models: i) adversarial stochastic noise and ii) depolarizing noise. In error model (i), each physical operation, or "location," in the quantum circuit (single-qubit preparation, quantum gate, memory step or single-qubit measurement) fails with probability at most ϵ . Noise is adversarial because the noise channel acting at each faulty physical operation can be arbitrary; noise can even be correlated across different faulty locations. Error model (ii) differs from model (i) in that the noise channel acting at each faulty location is the depolarizing channel: When a single-qubit (resp. two-qubit) location fails, then with probability $=4$ (resp. $=16$) the noise channel applies one of the 4 (resp. 16) Pauli operators with support on the qubits acted upon by the faulty location.

Adversarial stochastic noise is the natural form of noise to consider when analyzing fault-tolerant circuit simulations that use concatenated codes. This is because, even if the physical error model does not include correlations between different faulty physical operations, the effective noise that acts on all concatenation levels higher than the first one includes correlations which arise due to coding and the propagation of syndrome information [11]. Our threshold lower bounds for adversarial stochastic noise were obtained by performing a malignant-fault analysis on extended rectangles according to the method that was introduced in Ref. [11].

Our analysis for depolarizing noise differs from the analysis for adversarial noise only at the first coding level: For all coding levels other than the first one, we take the effective noise to be adversarial noise, thus clearly overestimating the effective noise correlations at these levels. For the first coding level, our malignant-fault analysis makes use of the fact that noise is depolarizing to obtain an improved upper bound on the probability of level-1 logical errors relative to the upper bound for adversarial noise. Our method gives rigorous lower bounds on the depolarizing threshold which exceed our rigorous threshold lower bounds for adversarial noise by up to 40% for some of the codes we have analysed.

Table I summarizes our results. We carried out the required combinatorial analysis for the concatenated $C_{BS}^{(3)}$ using SteFTEC and KnifTEC and for the concatenated $C_{BS}^{(5)}$ using SteFTEC. The analysis was done by using a computer program running on a cluster of 20 Pentium III processors. Our best rigorous lower bound on the

Code	Parameters	EC method	exact locs.	thr;adv	M-C	thr;adv	thr;depol	M-C	thr;depol
Steane	[[7,1,3]]	SteFTEC	575	2.73 10 ⁵	(1.21 0.06)	10 ⁴	1.60 10 ⁴	(1.60 0.02)	10 ⁴
	C _{B,S} ⁽³⁾ [[9,1,3]]	SteFTEC	297	1.21 10 ⁴					
C _{B,S} ⁽⁵⁾	[[25,1,5]]	SteFTEC	1,185	1.94 10 ⁴	(1.92 0.02)	10 ⁴	1.76 10 ⁴	(2.20 0.01)	10 ⁴
		KnFTEC	1,185						
Golay	[[23,1,7]]	SteFTEC	7,551		(2.07 0.03)	10 ⁴	(2.49 0.01)	10 ⁴	(2.49 0.01)
	C _{B,S} ⁽⁷⁾ [[49,1,7]]	SteFTEC	2,681						
		KnFTEC	2,681		(1.74 0.01)	10 ⁴	(1.78 0.01)	10 ⁴	
					(1.91 0.01)	10 ⁴	(1.98 0.01)	10 ⁴	

TABLE I: Rigorous lower bounds on the accuracy threshold with the concatenated Bacon-Shor code of varying block size and comparison with prior rigorous lower bounds using the concatenated Steane [[7,1,3]] [11] and Golay [[23,1,7]] [Reichardt, Ouyang; unpublished]. The fourth column gives the number of locations in the not extended rectangle [11]. The fifth column gives exact lower bounds on the threshold thr;adv for adversarial stochastic noise; the results are obtained using a computer-assisted combinatorial analysis. The sixth column is the Monte-Carlo estimate for thr;adv with 1 uncertainties. The seventh column gives exact lower bounds on the threshold thr;depol for depolarizing noise. The last column gives Monte-Carlo estimates of the threshold thr;depol for depolarizing noise. Bold fonts indicate the best results in each column.

accuracy threshold, $1.94 \cdot 10^{-4}$ for adversarial stochastic noise, was obtained for the concatenated $C_{B,S}^{(5)}$ using SteFTEC. This lower bound improves by nearly an order of magnitude the $2.73 \cdot 10^{-5}$ rigorous lower bound established in Ref. [11] with the concatenated Steane [[7,1,3]] using SteFTEC.

Analyzing codes of larger block size than $C_{B,S}^{(5)}$ proved to be computationally difficult in this exact setting. In these cases, we have used a Monte-Carlo malignant-fault analysis: We uniformly sample the set of fault paths with a fixed number of faults inside an extended rectangle and estimate what fraction \hat{f} of these sets leads to a logical error. This, in turn, gives an estimate of the exact combinatorial coefficients with a standard error $\hat{f}(1 - \hat{f})/N$ where N is the sample size. From these estimates on the combinatorial coefficients, we can then estimate the accuracy threshold as in the exact case. We have also applied this Monte-Carlo method to the cases where we could extract the exact combinatorics in order to provide evidence that the Monte-Carlo estimates are accurate; as can be seen in Table I, the exact threshold lower bounds in those cases lie within 1 of the estimated lower bounds. Our Monte-Carlo results for the variety of codes we have analysed give evidence that the accuracy threshold achieves a maximum over all members of the Bacon-Shor code family of $(2.07 \pm 0.03) \cdot 10^{-4}$ for adversarial stochastic noise and $(2.49 \pm 0.01) \cdot 10^{-4}$ for depolarizing noise, both obtained with the concatenated $C_{B,S}^{(5)}$ using KnFTEC. Section E in the Appendix discusses the details of our threshold analysis.

In conclusion, we have shown how the gauge freedom in the sub-system Bacon-Shor code can be exploited to design FTEC procedures with remarkable fault-tolerance properties. We have presented a new FTEC method using nearest-neighbor two-qubit measurements which does not require the preparation of entangled ancillary states. We expect this FTEC method to be advantageous for computation with geometric locality constraints such as

in ion-trap or solid-state schemes. On the other hand, standard FTEC methods can be implemented using ancillary states created out of tensor products of cat states, thus greatly reducing the complexity of ancilla encoding and verification. Our lower bound on the quantum accuracy threshold, $1.94 \cdot 10^{-4}$ for adversarial stochastic noise, is the best that has been rigorously proven so far and improves previous rigorous lower bounds by nearly an order of magnitude.

We are grateful to Ike Chuang, David DiVincenzo, Debbie Leung, John Preskill, Krysta Svore, and Barbara Terhal for helpful discussions and suggestions. AC thanks John Preskill for the invitation to the Caltech Institute for Quantum Information, where some of this work was done. PA is supported by the NSF under grant no. PHY-0456720. AC is partially supported by a research internship at IBM Watson Research Center.

- [1] P. Shor. In Proc. 37th Annual Symposium on Foundations of Computer Science, page 56, Los Alamitos, CA (1996). IEEE Computer Society Press.
- [2] see [1] and references therein.
- [3] E. Knill, R. Laflamme, and L. Viola. Phys. Rev. Lett. 84, 2525{2528 (2000).
- [4] E. Knill. arXive e-print quant-ph/0603252.
- [5] D. W. Roberts, R. Laflamme, D. Poulin, and M. Lesosky. arXive e-print quant-ph/0504189.
- [6] D. Bacon. Phys. Rev. A 73, 012340 (2006).
- [7] P. Shor. Phys. Rev. A 52, 2493{2496(R) (1995).
- [8] D. Gottesman. Ph.D. thesis, California Institute of Technology, Pasadena, CA (1997).
- [9] A. Steane. Phys. Rev. Lett. 78, 2252 (1997).
- [10] E. Knill. Nature 434, 39{44 (2005).
- [11] P. Aliferis, D. Gottesman, and J. Preskill. Quantum Inf. Comput. 6 (2), 97{165 (2006).

A . D E R I V I N G T H E B A C O N - S H O R C O D E

Starting from Shor's code

One natural way to derive $C_{BS}^{(n)}$ is by starting with Shor's distance- n code ($C_{Shor}^{(n)}$) [A1]. Let us call $C_Z^{(n)}$ the classical n -bit repetition code mapping the logical computation-basis state $|jki\rangle$ to $|jki^n\rangle = |jki\rangle (k \in \mathbb{Z}_2)$. The Hadamard-rotated n -bit repetition code $C_X^{(n)}$ maps the logical states $|j\rangle$ to $|j\rangle^{\otimes n}$, where $|j\rangle$ denote the 1 eigenvectors of the Pauli \times operator. Then, $C_{Shor}^{(n)}$ is the concatenated $C_Z^{(n)} \otimes C_X^{(n)}$ mapping the logical state $|jki\rangle$ to $|j^{\otimes n} i^{\otimes n} + (1)^k j^{\otimes n} i^{\otimes n}\rangle$, where $|j\rangle^{\otimes n} = |j\rangle^{\otimes n}$.

If we place the n^2 qubits in the $C_{\text{Shor}}^{(n)}$ block on the vertices of the $n \times n$ square lattice in Fig.1, then the code's stabilizer group is

$$S(C_{Shor}^{(n)}) = hX_{row\ i; row\ (i+1)}; \\ Z_{i;j}Z_{i;j+1}; Z_{n;j}Z_{n;j+1} \ j i; j 2 \ Z_{n-1}i; \quad (6)$$

The stabilizer in Eq. (6) fixes a two-dimensional subspace, the code space, encoding one logical qubit. The logical Pauli X and Z operators are respectively $X_{row\ 1}$ and $Z_{col\ 1}$.

By its construction, Shor's code treats X and Z errors asymmetrically: In each of the n rows, up to $b_n=2c$ X errors can be corrected because of the underlying classical repetition code. The code can also correct up to $b_n=2c$ Z errors on different rows; pairs of Z operators in the same row act trivially; the code is degenerate. As a first step towards removing this asymmetry, we observe that pairs of X operators in the same column commute with the logical Z operator. It would therefore be sufficient for successful error correction if we could restore zero parity for X errors in each given column instead of correcting X errors in each row separately.

Since only the parity of X errors in each column is relevant, we can replace the n stabilizer generators $Z_{i,j}Z_{i,j+1}$ for $i \in Z_n$ and j by their tensor-product $Z_{\text{col } j, \text{col } (j+1)}$. Repeating for all $j \in Z_n$, we reduce the stabilizer group of $C_{\text{Shor}}^{(n)}$ in Eq. (6) to the stabilizer group of $C_{BS}^{(n)}$ in Eq. (1).

Starting from Bravyi and Kitaev's surface code

We will also give an intriguing alternative derivation of $C_{BS}^{(n)}$ starting from Bravyi and Kitaev's distance- n surface code ($C_{BK}^{(n)}$) [A2]. If we place the $n^2 + (n-1)^2$ qubits in the $C_{BK}^{(n)}$ block on the edges of a square lattice as shown in Fig. 3, the code's stabilizer group is generated by X operators acting on all qubits neighboring a vertex ("site" operators) and Z operators acting on all qubits neighboring a vertex of the dual lattice ("plaquette" operators).

The logical operators are $X_L = X_{\text{row } 1}$ and $Z_L = Z_{\text{col } 1}$ and do not act on qubits with half-integer coordinates. It can easily be verified that, if all qubits with half-integer coordinates are measured in the computation basis, the remaining qubits are stabilized by $S (C_{BS}^{(n)})$. Moreover, the logical X and Z operators are not disturbed and match the logical operators for $C_{BS}^{(n)}$. This implies that the same state which was encoded in the $C_{BK}^{(n)}$ block is, after the measurements, encoded in $C_{BS}^{(n)}$.

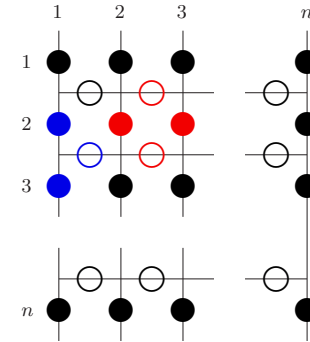


FIG. 3: (color online) Qubits in the $C_{B_K}^{(n)}$ block sit on the edges of a square lattice with different boundary conditions at top-bottom ("rough" edges) and left-right ("smooth" edges). Two elements of the code stabilizer are shown: X is applied on qubits shown in blue ("site" operator); Z is applied on qubits shown in red ("plaquette" operator). If all qubits shown as empty circles are measured in the computation basis, the remaining qubits will be encoded in $C_{B_S}^{(n)}$.

B . FTEC W ITH M EASUREMENTS ON THE GAUGE QUBITS

In Fig.2(a) (reproduced in Fig.4(a)) we showed a circuit for implementing the measurement of the operator $X_{j,i}X_{j+1,i}$ using one ancillary qubit. An alternative circuit for implementing the same measurement in smaller depth with respect to the data qubits is shown in Fig.4(b). It can easily be verified that the two circuits in Fig.4 are fault tolerant: In Fig.4(a), a fault in the $|j,i$ state can only propagate to $|j\rangle$ the measurement outcome but cannot harm the data. In Fig.4(b), a fault in the sub-circuit that prepares the ancillary Bell state can always be attributed to one of the two qubits (since $\begin{pmatrix} 0 & 1 \\ 1 & 0 \end{pmatrix} \begin{pmatrix} 0 & 1 \\ 1 & 0 \end{pmatrix}^T = \begin{pmatrix} 1 & 0 \\ 0 & 1 \end{pmatrix}$) and, hence, an error can only propagate to at most one qubit in the data. Consider now faults in the cnot gates acting on the data. In Fig.4(b), the gates are transversal so errors cannot spread from one data qubit to the other. In Fig.4(a), we might worry that there is a problem if the first cnot is faulty because an X error can result in both data qubits. But we soon realize that $X_{j,i}X_{j+1,i}$ is not an error! it is exactly the operator we are trying to

measure and so acts trivially after the measurement has taken place.

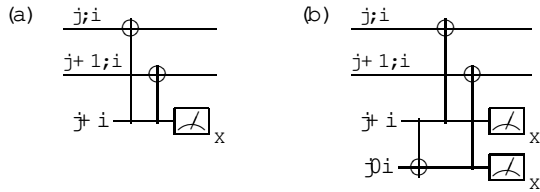


FIG. 4: (a) A circuit for measuring the operator $X_{j;i}X_{j+1;i}$ in depth two using one ancilla. (b) A circuit for implementing the same measurement in depth one using an ancillary Bell state. (Depth is measured with respect to the data qubits as ancillae can be prepared separately in order to be available exactly when needed.)

We should emphasize that, just as in the standard syndrome measurement procedure that uses cat states [1, A 3], the syndrome we obtain by using circuits as in Fig. 4 cannot in general be trusted unless some of the measurements are repeated. This redundancy is necessary since a single fault can cause errors in both the data block and the measurement outcomes. Overall, we need to check that the full FTEC circuit satisfies properties 0 and 1 in x9 in Ref. [11]. We will return to this point when we discuss specific examples in Section E in this Appendix.

A two-dimensional layout

Fig. 5 shows a simple example of a square-lattice architecture where data qubits in the $C_{BS}^{(3)}$ block are interspersed with ancillary qubits in a way that syndrome measurement can be implemented with nearest-neighbor interactions and only three qubit swaps. In the first round of FTEC, nine two-qubit ZZ operators are measured: Using superscripts to denote the data qubit acted by an operator, ancilla 1 in Fig. 5(b) is used to measure $Z^{(1)}Z^{(2)}$, ancilla 2 to measure $Z^{(1)}Z^{(3)}$ and ancilla 3 to measure $Z^{(1)}Z^{(2)}$ again (repetition of this measurement is necessary for fault tolerance). At the same time, similar measurements are performed on the other two rows. Next, the three qubit swaps indicated by ellipses in Fig. 5(b) are performed which result in interchanging the qubits in rows and columns. Finally, to complete the syndrome extraction, nine two-qubit XX operators are measured by coupling data and ancillary qubits as for the first round of measurements. In this paper, we have not carried out a threshold analysis in the geometrically local setting.

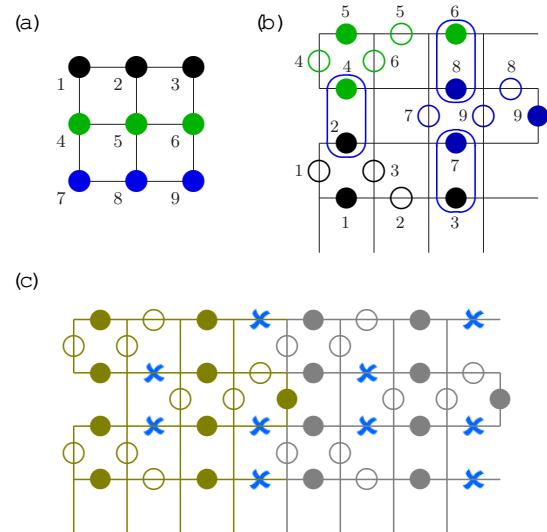
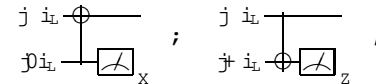


FIG. 5: (color online) (a) A color code for the qubits in the $C_{BS}^{(3)}$ block. (b) The block qubits are arranged on a square lattice interspersed with nine ancillary qubits shown as empty circles. The first round of FTEC consists of nearest-neighbor gates between data and ancillary qubits of the same color followed by measurements of the ancillae. Then, after the three qubit swap operations indicated by ellipses are performed, a similar sequence of nearest-neighbor gates and measurements is performed to complete the syndrome extraction. (c) Two $C_{BS}^{(3)}$ blocks side by side; e.g., these would be two of the nine sub-blocks within a code block at the second coding level when $C_{BS}^{(3)}$ is concatenated with itself. Sympathetic cooling ions, which may be needed for trapped-ion implementations, may be placed at the blue 'x' positions since these positions are not used during FTEC.

C. FTEC USING ENCODED ANCILLAE

SteFTEC

Recall that Steane's FTEC method (SteFTEC) [9], which applies to CSS codes, is based on the circuits



where j_{i_L} is the state of the input code block and j_{i_L} , j_{i_L} denote ancillary blocks encoded in the corresponding logical states in the same code as the data. The CNOT gates denote transversal CNOT gates acting between the data and ancilla blocks (the logical CNOT gate is transversal for CSS codes), and the measurements are understood as also being performed transversally. Evidently, as we would expect for error-correction circuitry, these circuits act trivially on the input encoded information. However, their non-trivial content is that the outcomes of the transversal measurements reveal the parity of the code syndromes in the input and ancilla blocks.

We have seen that one way to specify \mathcal{P}_{i_L} is via the stabilizer group in Eq. (5). In other words, our \mathcal{P}_{i_L} is the state

$$\mathcal{P}_{i_L} = \bigotimes_{j=1}^{O^n} \frac{j+ + \text{cnot}_{i_L} + j}{2}^{\text{row}_{i_L}} ; \quad (7)$$

where inside the parenthesis we have the state of the n qubits in column n j in Fig.1, and we have taken the tensor product of n identical such states on each one of the n columns. Similarly, our \mathcal{P}_{i_L} is the state

$$\mathcal{P}_{i_L} = \bigotimes_{i=1}^{O^n} \frac{\mathcal{P}_0 + \text{row}_{i_L} + \text{row}_{i_L}}{2}^{\text{row}_{i_L}} ; \quad (8)$$

Standard circuits for encoding the states in Eqs. (7) and (8) will be shown in Section E in this Appendix. We observe that the Hadamard-rotated cat states in Eq. (7) need only be verified [1] against multiple correlated Z errors but not against correlated X errors (any pair of X errors acts trivially on the state in Eq. (7)). This implies that, instead of Z-error verification, repetition of the syndrome measurement using different \mathcal{P}_{i_L} ancillary blocks is sufficient for fault tolerance. This is because only X errors can propagate from the \mathcal{P}_{i_L} block to the data due to the direction of the cnot gates, while here no correlated X errors can appear in \mathcal{P}_{i_L} . Similar observations hold for \mathcal{P}_{i_L} for which verification against correlated X errors can be avoided if we repeat the syndrome measurement.

KnifTEC

Knill's FTEC method (KnifTEC) [10], shown schematically in Fig.6 for $C_{BS}^{(n)}$, is more general than SteFTEC as it applies to any stabilizer code. In Fig.6, an ancillary logical Bell state ($|j_0 i_L\rangle$) is prepared and then transversal Bell measurements are performed between the input code block and one half of this ancilla. Finally, a logical Pauli operator P_r is applied on the output code block in order to complete the logical teleportation of the input code state.

As in SteFTEC, the outcomes of the transversal measurements reveal the parity of the code syndromes in the input block and the half of the $|j_0 i_L\rangle$ ancilla that is being measured. First, this syndrome information allows us to perform error correction on the measurement outcomes. Then, we can compute parities on the, now corrected, measurement outcomes in order to obtain the eigenvalues of the logical X and Z operators acting on the input code block and the half of the $|j_0 i_L\rangle$ ancilla that was measured. Because both the input block and the logical Bell state are encoded in the same code, knowing the eigenvalues for these two logical operators allows us to complete the logical teleportation of the input code state by applying the appropriate logical Pauli correction

P_r on the output code block. As usual, P_r need not actually be applied but can be kept in a classical memory as long as the succeeding logical operations are in the Clifford group [10].

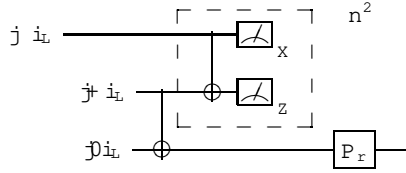


FIG.6: A schematic of KnifTEC for a code with n^2 qubits in the code block such as $C_{BS}^{(n)}$. An ancillary logical Bell state is first prepared before transversal Bell measurements are done between the input code block and one half of the ancilla. The measurement outcomes are constrained by parities which enable error correction. Then, the corrected measurement outcomes allow us to determine the logical Pauli operator P_r necessary to complete the logical teleportation of the input code state $j_0 i_L$.

A remarkable feature of this FTEC method is that faults in the execution of the transversal Bell measurements can only result in an error in the logical Pauli operator P_r if the logical Bell state is prepared without faults, the output code block is always in the code space independent of whether faults occurred in the transversal Bell measurements. The value of this observation comes when we consider performing a malignant-fault analysis inside an extended rectangle [11] where KnifTEC is used. Consider the leading KnifTEC gadgets inside the extended rectangle and let faults occur somewhere in the transversal Bell measurements. As we noted, these faults can only cause an error in P_r but cannot take the output code block outside the code space. Hence, these faults cannot combine with other faults elsewhere in the extended rectangle to cause a logical error and a crash of the computation. Therefore, for the purposes of malignant-fault analysis, the transversal Bell measurements in the leading KnifTEC gadgets in an extended rectangle can be taken as ideal. This reduces the number of locations that need to be considered in a malignant-fault analysis and sheds light onto why KnifTEC performs better than SteFTEC for all codes analysed in Table I.

D. UNIVERSAL QUANTUM COMPUTATION

We have already discussed that, since the stabilizer generators in Eq. (1) consist of either tensor products of X operators alone or tensor products of Z operators alone, the Bacon-Shor code belongs to the CSS family of quantum codes. Therefore, the logical cnot operation is transversal: If we imagine bringing two square lattices as in Fig.1 one on top of the other, applying cnot gates between will result in a logical cnot between the two protected logical qubits.

In addition, the logical H adam ard is also transversal up to a 90-degree rotation of the lattice. By combining the logical cnot with the logical H adam ard, we find that the logical cphase is also transversal since it can be implemented by doing a logical H adam ard on the target, followed by a logical cnot, followed by another logical H adam ard on the target. This implies that the logical cphase can be implemented transversally between two code blocks by i) rotating by 90 degrees the lattice of one, say the second, code block, ii) interacting the qubits in the two lattices bitwise with cphase gates, and iii) performing another 90-degree rotation of the lattice of the second code block.

A destructive measurement of the logical X (resp. Z) operator can be performed by transversally measuring the operator X (resp. Z) on each qubit in the code block. (With the logical cnot and cphase transversal, we can also measure non-destructively the logical X or the logical Z operator by using as control an ancilla prepared in the logical $|j ii\rangle$ state.) If we were also able to easily measure the logical $Y = iXZ$ operator (Y_L), we would be able, using e.g. the circuit in Fig. 7, to implement the logical phase gate $S = \exp(-i\frac{\pi}{4}Z)$. The logical cnot, H adam ard and phase gates would then be sufficient for generating the logical C li ord group in a fault-tolerant manner.

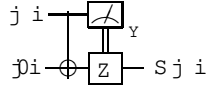


FIG. 7: Circuit simulation of the phase gate S using a measurement of Y .

Although $Y_L = \bigotimes_{i=1}^n Y^{(i)}$ for n odd, measuring transversally the operators $Y^{(i)}$ does not give a fault-tolerant measurement of Y_L . This is because the Bacon-Shor code has no stabilizer operators which can be written as tensor products of Y operators alone. Therefore, the problem is that we cannot perform error correction on the transversal measurement outcomes and, so, the eigenvalue we would deduce for the logical Y could be erroneous even if a single one of the transversal measurements failed.

We could instead measure the logical Y operator non-destructively using cat states [1, A 3]. Implementing this measurement would require controlled- Y gates which, at the next level of concatenation, would have to be implemented in an encoded form. But then, the problem is that the controlled- Y gate is complex and all the transversal operations we have discussed so far (cnot, cphase and H adam ard) are real. Hence, we don't have a direct fault-tolerant method for implementing the logical controlled- Y gate.

Fortunately, as we will discuss next, there is a method for simulating the logical S gate by using only logical cnot and cphase gates provided we can fault-tolerantly

prepare a certain logical ancillary state. To complete quantum universality, we also need to simulate some logical gate outside the C li ord group | we will take this to be the To oli gate or some real non-C li ord rotation.

We will next describe how the logical S and To oli gates can be simulated fault-tolerantly in the Bacon-Shor code. Our discussion is borrowed from the universality construction for the Bravyi-Kitaev surface code in Ref. [A 4]. The fact that universality can be achieved in the same way for these two codes is not surprising; as we discussed in Section A of this Appendix, the Bacon-Shor code can be viewed as a reduction of the Bravyi-Kitaev surface code after some qubits that do not enter into the logical operations of the code have been measured.

The logical S gate

Consider the states $|j ii\rangle = \frac{1}{\sqrt{2}}(|j i\rangle + |i j\rangle)$ which are the $|1\rangle$ eigenstates of Y . Given the state $|j ii\rangle$, we can simulate S (up to an irrelevant phase) on some input state $|j i\rangle$ using the circuit in Fig. 8. Furthermore, if the state $|j ii\rangle$ is used instead in the same circuit, then the operation $S^Y = S$ will be simulated. Since the logical cnot and cphase can be implemented transversely, the problem of simulating the logical S gate fault-tolerantly reduces to the problem of fault-tolerantly preparing the logical ancillary state $|j ii\rangle$ or $|j ii\rangle$.

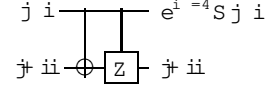


FIG. 8: Circuit simulation of the phase gate S using the ancillary state $|j ii\rangle$.

Simulating S and S^Y in superposition

Based on the circuit in Fig. 8, we will now first describe a surprisingly simple procedure by which the simulation of the logical S gate is still possible even if the logical ancillary state $|j ii\rangle$ is replaced by another logical ancillary state which is easier to prepare [A 4]. This procedure makes use of the fact that the S gate is the only complex gate in our universal gate set.

Consider using some standard state, say the state $|j i\rangle$, instead of $|j ii\rangle$ in the circuit in Fig. 8. We can expand $|j i\rangle = \frac{1}{\sqrt{2}}(|j ii\rangle + |i j\rangle)$ and, for each of the two terms, we can consider the two paths of the subsequent computation which are executed in superposition. In one path S is simulated and in the other S^Y . Thus, if every time we want to simulate S in our circuit we use the same ancillary $|j i\rangle$ state and because S is the only complex gate in our gate set, the final state of the computation will be a

linear superposition of one term where the desired computation unitary U has been implemented and a second term where U has been implemented instead. In other words, if the initial computation state is $|j_{\text{initial}}\rangle$, then the final computation state will be

$$|j_{\text{final}}\rangle = \frac{|j_{\text{ii}}\rangle U |j_{\text{initial}}\rangle + |j_{\text{ii}}\rangle U^\dagger |j_{\text{initial}}\rangle}{\sqrt{2}} : \quad (9)$$

In the end of the computation some operator A will be measured which we can take to be real (and so, due to hermiticity, $A^\dagger = A$). We now want to see that the expectation value for A will be the same as if the desired U had been simulated all along. Indeed, we compute

$$\begin{aligned} hA|i\rangle &= h|j_{\text{initial}}\rangle \frac{|U^\dagger A U + (U^\dagger)^* A U}{2} |j_{\text{initial}}\rangle \\ &= h|j_{\text{initial}}\rangle U^\dagger A U |j_{\text{initial}}\rangle; \end{aligned} \quad (10)$$

since, $h|j_i\rangle h|j(U^\dagger A U) j_i\rangle = h|j^\dagger U^\dagger A^\dagger U j_i\rangle = h|j^\dagger A j_i\rangle$.

We can use this procedure at the logical level as well. The only penalty we pay for simulating the logical S gate in this way is that we need to swap around the ancillary $|j_{\text{pi}}\rangle$ block we use for the simulation if we are constrained to use only local interactions. But this will only give us a linear penalty in the size of the computation. Of course, we should emphasize that this trick works because the S gate is not used in implementing error correction and, as a consequence, it is not necessary that we execute different S gates in parallel anywhere in our computation. In addition, since the simulation uses only cnot and cphase gates and the preparation of the $|j_{\text{pi}}\rangle$ state, the logical S gate does not need to be considered separately in our analysis for determining the accuracy threshold.

Noisy $|j_{\text{ii}}$ purification

If we had not read Ref. [A 4] to know about the previous trick, there are also straightforward procedures for fault-tolerantly preparing the state $|j_{\text{ii}}\rangle$. For instance, we can begin by preparing many noisy logical $|j_{\text{ii}}$ states (e.g., by using teleportation to inject a single-qubit $|j_{\text{ii}}$ state into a code block [10]) and subsequently purify them. A possible purification circuit is shown in Fig. 9.

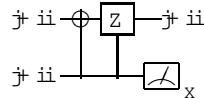


FIG. 9: Circuit for the non-deterministic purification of the $|j_{\text{ii}}$ state. Post-selecting on the measurement outcome being 1, the output $|j_{\text{ii}}$ state has quadratically improved fidelity.

The measurement outcome in the circuit above is ideally 1, and an error on one of the two $|j_{\text{ii}}$ states can be detected. We note that, because Y stabilizes the state

$|j_{\text{ii}}$, we need only worry about Z errors| we can write $X = iZ Y$ which is, up to the irrelevant phase i , equivalent to Z when it acts on $|j_{\text{ii}}$. Post-selecting on the measurement outcome in the circuit in Fig. 9 being 1, the fidelity of the output $|j_{\text{ii}}$ state is increased quadratically relative to the fidelity of the input states| it takes errors in both input $|j_{\text{ii}}$ states for an error in the output state to go undetected.

The purification procedure can also be implemented deterministically using the circuit in Fig. 10, this time using three input $|j_{\text{ii}}$ states. Ideally both measurements outcomes in this circuit give outcome 1. If both outcomes are +1 then, to first order in the error parameter, a Z error has occurred on the first $|j_{\text{ii}}$ state and, hence, a Z correction must be applied on the output state to invert it. The fidelity of the output $|j_{\text{ii}}$ state is again improved quadratically relative to the fidelity of the input states after one execution of the protocol.

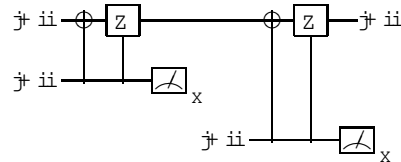


FIG. 10: The deterministic counterpart of the purification circuit in Fig. 9. A Z correction is applied on the output $|j_{\text{ii}}$ state if both measurement outcomes are +1, else no correction is applied. Again, the fidelity of the output is improved quadratically after one run of the protocol.

The logical Tooli gate

The simulation of the logical Tooli gate uses the logical ancillary state $|j_{\text{Tooli}}\rangle = |j_1\rangle |j_2\rangle |j_3\rangle$ in the circuit in Fig. 11 [1, A 5]. Depending on the measurement outcomes $j_{f1,2,3g} = 1$, the post-measurement Cli ord-group corrections are $X^{(1)} \text{cnot}_{2,3}$ if $k_1 = 1$, $X^{(2)} \text{cnot}_{1,3}$ if $k_2 = 1$, and $\text{cphase}_{1,2} Z^{(3)}$ if $k_3 = 1$, where $k_{f1,2,3g} = (1 - j_{f1,2,3g})/2 = 1$.

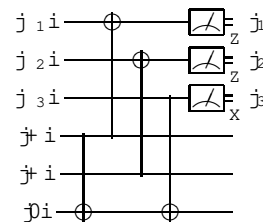


FIG. 11: Circuit simulation of the Tooli gate using the ancilla $|j_{\text{Tooli}}\rangle$. The post-measurement Cli ord-group corrections that depend on the measurement outcomes are not shown.

Therefore, as in the simulation of the logical S gate, the problem of simulating the logical Tooli gate fault-

tolerantly reduces to fault-tolerantly preparing a logical ancillary state, the logical $\text{J}\ddot{\text{o}} \text{oli}$.

Noisy $\text{J}\ddot{\text{o}} \text{oli}$ preparation by concatenation

$\text{J}\ddot{\text{o}} \text{oli}$ is the $+1$ eigenstate of the three operators $S_1 = X^{(1)} \text{cnot}_{2!3}$, $S_2 = X^{(2)} \text{cnot}_{1!3}$ and $S_3 = \text{cphase}_{1,2} Z^{(3)}$. Then, consider starting with the state $\text{J}\ddot{\text{i}}^3$ which is clearly a $+1$ eigenstate of both S_1 and S_2 . To obtain the state $\text{J}\ddot{\text{o}} \text{oli}$ it now remains to perform a measurement of the operator S_3 . This can be accomplished with the circuit in Fig.12 [A 5].

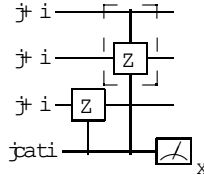


FIG. 12: A circuit that projects the input state $\text{J}\ddot{\text{i}}^3$ onto the $+1$ eigenstate of the operator S_3 depending on the measurement outcome. For outcome $+1$ the output state is $\text{J}\ddot{\text{o}} \text{oli}$.

If this circuit were executed in an un-encoded form, then the cat state would simply be one qubit in the state $\text{J}\ddot{\text{i}}$. However, the logical circuit will be executed instead and, then, the cat state is $\text{J}\ddot{\text{i}} / \text{J}\ddot{\text{o}} + \text{J}\ddot{\text{l}}$, i.e., the logical $\text{J}\ddot{\text{i}}$ state in the n^2 -bit classical repetition code $C_z^{(n^2)}$. The cat state must either be verified against X errors, or a decoding circuit can replace the transversal measurements in order to avoid verification [A 6]. To ensure fault tolerance, the measurement of the logical S_3 must be repeated in order to verify the measured eigenvalue.

Since the circuit in Fig.12 is realized in an encoded form, the first three states are logical $\text{J}\ddot{\text{i}}$ states and logical cphase and controlled-controlled-Z gates need be performed. Then, we observe that the logical controlled-controlled-Z gate (${}^2(Z)$) can be implemented using transversal ${}^2(Z)$ gates since the cphase is transversal; the qubits in one of the first two code blocks need to be rotated by 90 degrees before bitwise ${}^2(Z)$ gates are applied and then the qubits need to be rotated back by 90 degrees. Conjugating with bitwise Hadamard gates on the cat-state qubits, the bitwise ${}^2(Z)$ gates become bitwise $\text{J}\ddot{\text{o}} \text{oli}$ gates which allows this same circuit to be executed in a higher coding level as well.

The above procedure requires concatenation in order to increase the delity of the ancilla $\text{J}\ddot{\text{o}} \text{oli}$. To improve the accuracy threshold below which concatenation will reduce the logical error rate of this state, we can bootstrap the $\text{J}\ddot{\text{o}} \text{oli}$ preparation in Fig.12 to start at a higher coding level than the first coding level. That is, we can implement the $\text{J}\ddot{\text{o}} \text{oli}$ gates in the circuit in Fig.12 at a sufficiently high level of concatenation using

the simulation circuit in Fig.11 and to olig ancillae prepared, e.g., by state-injection [10]. Although these logical ancillae will have an error rate of the order of the physical error rate, the logical error rates of all C li ord-group operations in the circuits in Figs.11 and 12 can be made arbitrarily small provided we operate below the threshold of C li ord-group computation. Because of this, the accuracy threshold for the $\text{J}\ddot{\text{o}} \text{oli}$ preparation will be significantly higher than the threshold for C li ord-group gates which, therefore, will set the overall accuracy threshold.

Noisy $\text{J}\ddot{\text{o}} \text{oli}$ purification

As an alternative to concatenation, we can consider preparing several copies of the logical $\text{J}\ddot{\text{o}} \text{oli}$ state (again, by using, e.g., state-injection [10]) and purifying them [A 7, A 8]. First, let us construct a circuit that takes as an input some number of copies of the $\text{J}\ddot{\text{o}} \text{oli}$ state and outputs one $\text{J}\ddot{\text{o}} \text{oli}$ state of improved delity.

Consider the circuit in Fig.13. We start with one copy of the state $\text{J}\ddot{\text{o}} \text{oli}$ and measure the operator S_1 using one ancillary qubit initialized in the state $\text{J}\ddot{\text{i}}$. Since the state $\text{J}\ddot{\text{o}} \text{oli}$ is an eigenstate of this operator, the effect of the measurement is trivial: the first three qubits remain in the state $\text{J}\ddot{\text{o}} \text{oli}$ and the measurement on the ancilla always ideally gives outcome $+1$.

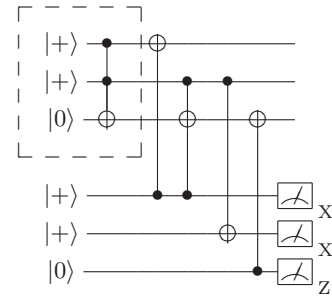


FIG. 13: A circuit that uses one ancillary qubit to measure the operator $S_1 = X^{(2)} \text{cnot}_{1!3}$ on the input $\text{J}\ddot{\text{o}} \text{oli}$ state. The measurement outcome is ideally $+1$ since $\text{J}\ddot{\text{o}} \text{oli}$ is an eigenstate of S_1 . Note that the gates acting on the second and third ancillae operate trivially.

The circuit in Fig.13 includes two extra ancillae. These qubits are useful because we now want to insert two cancelling To olig gates acting on the ancillae in this circuit. We thus obtain the equivalent circuit shown in Fig.14. Our motivation for inserting the resolution of the identity in the form of the two To olig gates is to create two copies of the state $\text{J}\ddot{\text{o}} \text{oli}$ in the input of the circuit. Thus, we next commute the leftmost of the two To olig gates to the left of the circuit using repeatedly the circuit identities in Fig.15. After the dust settles, the result is the circuit shown in Fig.16.

The circuit in Fig.16 includes, except for the two input $\text{J}\ddot{\text{o}} \text{oli}$ states, additional To olig gates acting between

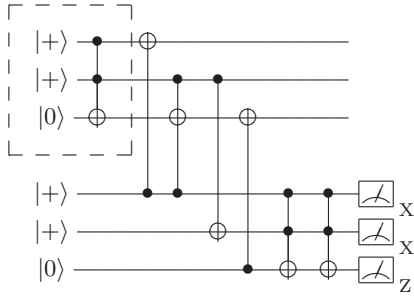


FIG. 14: The circuit in Fig.13 where a pair of cancelling Toffoli gates have been inserted.

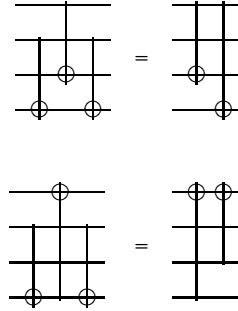


FIG. 15: Commutation relations of cnot and Toffoli.

these two states which we do not know how to perform fault-tolerantly | recall that our goal is to design a purification circuit for the $\text{J}\ddot{\text{o}}\text{olii}$ state that uses exclusively Clifford-group operations. However, if we measure the last two qubits in this circuit as shown in Fig.17, we can apply corrections depending on the measurement outcomes that will restore the state of the first three qubits to be the $\text{J}\ddot{\text{o}}\text{olii}$ state.

Furthermore, if we subsequently measure the fourth qubit, we will obtain the product of the eigenvalues of S_1 acting on the two input $\text{J}\ddot{\text{o}}\text{olii}$ states. Ideally this product is +1 because both input $\text{J}\ddot{\text{o}}\text{olii}$ states are eigenstates of S_1 . Hence, if the measured product is 1, we know that one of the input $\text{J}\ddot{\text{o}}\text{olii}$ states had an error. In that case we can either reject both copies and start over or, to make the purification procedure deterministic, we can use a third copy of the $\text{J}\ddot{\text{o}}\text{olii}$ state and compare the surviving copy from this round of purification with this new $\text{J}\ddot{\text{o}}\text{olii}$ state. If a 1 product is measured again, then we know that, to first order in the error parameter, the error has occurred on the first $\text{J}\ddot{\text{o}}\text{olii}$ copy and we can proceed to correct it. Otherwise, we become more confident that the first $\text{J}\ddot{\text{o}}\text{olii}$ copy is an eigenstate of S_1 as desired. Overall, by using either the deterministic or the non-deterministic purification procedure, the fidelity of the output $\text{J}\ddot{\text{o}}\text{olii}$ state improves.

In more detail, the 2^3 eigenstates of the three commuting operators S_1 , S_2 and S_3 form an orthonormal basis in the three-qubit Hilbert space. Moreover, the

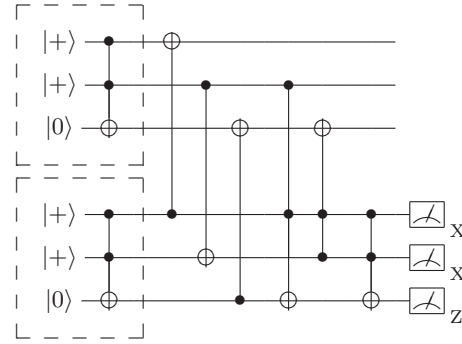


FIG. 16: An equivalent circuit to that in Fig.13. We identify the input to be two copies of the state $\text{J}\ddot{\text{o}}\text{olii}$ shown in boxes.

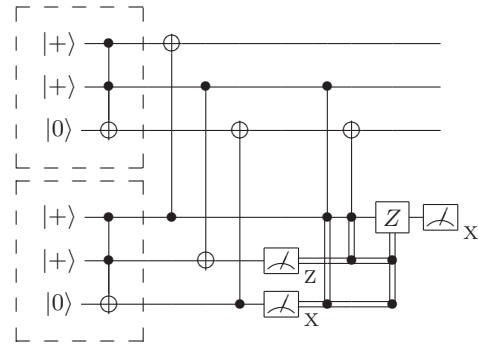


FIG. 17: After measuring the last two qubits in Fig.16 and applying the appropriate corrections, the first three qubits are left in the state $\text{J}\ddot{\text{o}}\text{olii}$. The fourth qubit is then measured with the outcome giving the product of the eigenvalues of S_1 acting in the two input $\text{J}\ddot{\text{o}}\text{olii}$ states.

state $\text{J}\ddot{\text{o}}\text{olii}$ that we want to purify is the +1 eigenstate of these operators; it is, therefore, one of the basis states in this basis. We can label any state in this basis by three numbers $a; b; c = \pm 1$ corresponding to its eigenvalues with respect to the operators S_1 , S_2 and S_3 . Let a basis state with parameters $a; b; c$ be denoted $\text{J}\ddot{\text{o}}\text{olii}_{a; b; c}$. Then, if the input to the purification circuit in Fig.17 is the two states $\text{J}\ddot{\text{o}}\text{olii}_{a; b; c}$ and $\text{J}\ddot{\text{o}}\text{olii}_{a^0; b^0; c^0}$, the first three qubits at the output are in the state $\text{J}\ddot{\text{o}}\text{olii}_{a; b; c}$. Moreover, the measurement outcome on the fourth qubit corresponds to a $\frac{a}{b}c$; i.e., it equals the product of the eigenvalues of S_1 of the two input copies.

Thus, the circuit in Fig.17 proves the fidelity of the surviving state $\text{J}\ddot{\text{o}}\text{olii}_{a; b; c}$ with respect to the parameter a , but the parameters b and c get worse | if any one of the input copies was a ± 1 eigenstate of S_2 or S_3 , then the surviving copy will also be such a ± 1 eigenstate. However, the fidelity with respect to the parameters b and c only gets worse by a linear factor whereas the fidelity with respect to a improves quadratically [A 7, A 8]. Therefore, if we repeat the purification protocol using another circuit that purifies with respect to the b parameter and also with a third circuit that purifies with respect to c ,

we will achieve a quadratic improvement in the fidelity with respect to all three parameters a , b and c . Such circuits can be constructed using a similar trick as the one we used to derive the circuit in Fig.17 from that in Fig.13.

A lternative paths to universality

The logical T_y gate

Instead of the T₀ gate, we could use the real non-Clifford gate $T_y = \exp(-i\frac{\pi}{4}y)$ to obtain a quantum universal gate set. To simulate T_y it is sufficient to prepare the $+\frac{1}{2}$ eigenstate of the Hadamard gate, $\frac{1}{2}(\cos(\frac{\pi}{4})|0\rangle + \sin(\frac{\pi}{4})|1\rangle)$, and use the circuit in Fig.18.

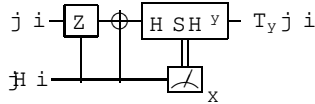


FIG.18: Circuit simulation of the gate T_y using the ancillary state $|0\rangle$.

The purification of the ancilla $|0\rangle$ can be done nondeterministically as discussed in Refs. [A 9] and [A 10]. Assuming Clifford-group gates are ideal, the threshold accuracy for $|0\rangle$ distillation is at least $1 - 0.927^2 = 14\%$ [A 10], which is significantly higher than the accuracy threshold for Clifford-group operations.

Bootstrapping another code with transversal logical S gate

Alternatively, we could use the Bacon-Shor code for the initial levels of concatenation only and then bootstrap another code with more convenient universality properties. For example, the Bacon-Shor code could be concatenated sufficiently many times until the logical error rate for the cnot, Hadamard gates and $|0\rangle$, $|1\rangle$ preparation at the top level becomes significantly lower than the threshold for the $[[7;1;3]]$ code for which the logical S gate is transversal. At the first level where the new bootstrapped code is to be used, ancillae that enable the simulation of the logical S and the non-Clifford $T = S^{1/2}$ gates at the top level of the concatenated Bacon-Shor code could be constructed using e.g. state-injection [10].

E. ACCURACY THRESHOLD LOWER BOUNDS

The $[[4,1,2]] C_{BS}^{(2)}$ code

$C_{BS}^{(2)}$ is a one error detecting code with stabilizer group and logical operators in H_L and H_T , respectively,

$$\begin{aligned} S(C_{BS}^{(2)}) &= hX_{row\ 1;row\ 2}; Z_{col\ 1;col\ 2}i; \\ L &= fX_{row\ 1}; Z_{col\ 1}g; \\ T &= fX_{col\ 1}; Z_{row\ 1}g; \end{aligned} \quad (11)$$

For this code, SteFTEC and FTEC by measurements on the gauge qubits are identical in the following sense: Consider our logical $|0\rangle$ state. It consists of two Hadamard-rotated cat states aligned along the two columns. But, a two-qubit cat state is the same as a Bell state and Bell states are the same in the computation and in the Hadamard-rotated basis. Thus, a measurement of the syndrome using a $|0\rangle$ ancilla is the same as running the circuit in Fig.4(b) in parallel in the two columns for the measurement of $X_{1,1}X_{2,1}$ and $X_{1,2}X_{2,2}$. Clearly, by combining the outcomes of these two measurements, we can deduce the eigenvalue of the stabilizer generator $X_{row\ 1;row\ 2}$. Doing a similar measurement across the two rows will give us the eigenvalue of the other stabilizer generator $Z_{col\ 1;col\ 2}$.

Because $C_{BS}^{(2)}$ only enables error detection, techniques based on postselection similar to those discussed in Refs. [10, A 9] are necessary to obtain an accuracy threshold by concatenation. We have not analysed such a scheme in this paper.

The $[[9,1,3]] C_{BS}^{(3)}$ code

$C_{BS}^{(3)}$ is a one error correcting code with stabilizer group

$$\begin{aligned} S(C_{BS}^{(3)}) &= hX_{row\ 1;row\ 2}; X_{row\ 2;row\ 3}; \\ &Z_{col\ 1;col\ 2}; Z_{col\ 2;col\ 3}i; \end{aligned} \quad (12)$$

The encoded operations in H_L are again $X = X_{row\ 1}$ and $Z = Z_{col\ 1}$. As in Eq. (3), the group T is generated by operators with an even number of Z operators in each row and an even number of X operators in each column.

Circuits for FTEC using measurements on the gauge qubits are shown in Fig.19. The advantage of this method is that ancillary qubits initialized in a product state are sufficient for extracting the syndrome information. However, we note that more cnot gates acting on the data qubits are necessary than with SteFTEC or KnFTEC (circuits for these FTEC methods will be shown next). Because, e.g., a Z error on both qubits acted upon by the second cnot operating on qubit $(2;j)$ will flip the eigenvalue of the measured operator $X_{1;j}X_{2;j}$.

and also create a $Z_{2;j}$ error in the data, the measurement of an extra operator is necessary for fault tolerance [A 12]; in Fig.19 we have chosen to measure the extra operator $X_{1;j}X_{3;j}$. This extra measurement provides the necessary redundancy in order to avoid having one fault cause a logical error in the data block.

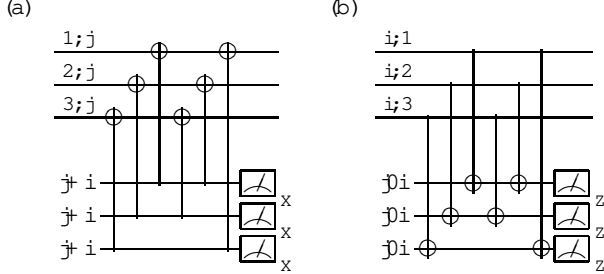


FIG . 19: FTEC for $C_B^{(3)}$ using measurements on the gauge qubits. (a) Measuring operators in T along column j . (b) Measuring operators in T along row i . Identical circuits are run in parallel for all rows and columns. In both circuits, the third measurement is used to provide an extra redundancy bit for fault tolerance. For maximum qubit efficiency, all measurements could be implemented sequentially using the same ancillary qubit.

For SteFTEC, in order to measure the syndrome for Z errors we need to prepare a logical $\tilde{\rho}_i$ state which consists of three Hadamard-rotated cat states aligned across the three columns. For column j the circuit is therefore as in Fig.20(a). To obtain the syndrome for X errors, we prepare a logical $\tilde{\rho}_i$ state which consists of cat states along the three rows. For row i the circuit is shown in Fig.20(b). We observe that these circuits have the remarkable property that they are fault tolerant without the need to verify the different cat states. Indeed, consider a faulty cnot inside the encoding circuit for these cat states. A X error on both qubits acted upon by this gate is either i) an operator in the cat-state stabilizer in Fig.20(a) or, ii) is equivalent to a single X error on the other qubit in Fig.20(b). Similarly for a Z error acting on both qubits. Otherwise, a X error acting on one qubit and a Z error on the other cannot lead to more than one X and/or one Z error propagating from the cat state to the data block. Thus, properties 0, 1 in Ref. [11] are satisfied [A 11].

The circuitry for KnFTEC also uses three-qubit cat states and transversal cnot gates for preparing a logical Bell state. As with the encoded ancillae for SteFTEC, this preparation circuit for the logical Bell state is also fault tolerant without the need for ancilla verification. Moreover, the circuits for SteFTEC and KnFTEC contain exactly the same number of locations.

A crude lower bound on the accuracy threshold can be obtained by counting the total number of fault pairs inside the cnot extended rectangle [11]. The SteFTEC circuit contains 72 qubit-preparation, measurement, gate or

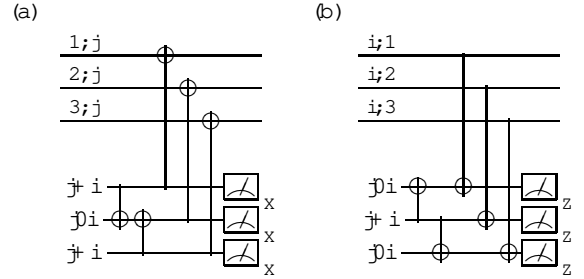


FIG . 20: SteFTEC for $C_B^{(3)}$. (a) Collecting the syndrome for Z errors. The circuit in column $n j$ is shown. (b) Collecting the syndrome for X errors. Here, the circuit for row i is shown. Identical circuits are run in parallel for all three rows and columns.

memory locations. The cnot extended rectangle therefore contains $4 \cdot 72 + 9 = 297$ locations. This yields a threshold lower bound of $\frac{297}{2}^{1/2} \cdot 2 \cdot 2 \cdot 10^{-5}$.

Let us denote by i the error strength (probability or amplitude, depending on the error model) for location type i , where locations are labeled as (1) memory, (2) $\tilde{\rho}_i$ preparation, (3) $\tilde{\rho}_i$ preparation, (4) measurement of X , (5) measurement of Z and (6) cnot. A detailed analysis of malignant pairs of faults [11] using SteFTEC gives for the error probability of the level- k cnot extended rectangle:

$$\frac{(k)}{6}^{X^6} \sum_{i,j} \frac{(k-1)}{i} \frac{(k-1)}{j} + B_6 \left(\frac{(k-1)}{\max} \right)^3; \quad (13)$$

where $\frac{(k-1)}{\max} = \max_i \frac{(k-1)}{i}$ (with our choice of a quantum universal gate set, $\frac{(k-1)}{\max} = \frac{(k-1)}{6}$). Third or higher order events contribute $B_6 = \frac{297}{3} \cdot 4 \cdot 32 \cdot 10^6$ and the coefficients i_j were found by a computer-assisted combinatorial analysis to be

$$\begin{array}{ccccccccc} 0 & & & & & & & & 1 \\ & 52 & & & & & & & \\ \frac{B}{B} & 174 & 138 & & & & & & \frac{C}{C} \\ \frac{B}{B} & 174 & 0 & 138 & & & & & \frac{C}{C} \\ \frac{B}{B} & 234 & 0 & 378 & 216 & & & & \frac{C}{C} \\ @ & 234 & 378 & 0 & 0 & 216 & & & \frac{A}{A} \\ & & & & & & & & \\ & 1154 & 1281 & 1281 & 1566 & 1556 & 3733 & & \end{array} \quad (14)$$

Taking all error rates equal, we obtain $A_6 = 12,913$ malignant pairs, or

$$\frac{(k)}{6}^{A_6^0} \frac{(k-1)}{6}^2; \quad (15)$$

where $A_6^0 = \frac{A_6}{2} \cdot 1 + \frac{q}{1 + \frac{4B_6}{A_6^2}} = 13,240$. This indicates $7.55 \cdot 10^{-5}$ as a lower bound on the accuracy threshold.

This lower bound can be improved further if we use the idea of "stretched" extended rectangles, i.e., if we omit FTEC steps at levels $k \geq 2$ wherever they are not necessary [A 13]. In particular, we can "stretch"

state preparation extended rectangles and join them with the succeeding cnot extended rectangles and, similarly, "stretch" measurement extended rectangles to join them with the preceding cnot extended rectangles. Then, for all levels $k \geq 2$, we need not consider separate preparation or measurement extended rectangles at level $k-1$. Instead, we can consider level- $(k-1)$ stretched extended rectangles that contain level- $(k-1)$ preparation (resp. measurement) joined with the succeeding (resp. preceding) level- $(k-1)$ cnot operations and the intermediate level- $(k-1)$ FTEC omitted. We observe that such stretched extended rectangles have error rates no worse than standard cnot extended rectangles because i) error correction following state preparation is superfluous as long as the encoding circuit is made fault tolerant using, e.g., state verification, and ii) measurement is performed transversally and so classical error correction on the measurement outcomes can replace quantum error correction preceding the measurements.

Thus, for levels $k \geq 2$, we can effectively set those coefficients in Eq. (14) that involve preparation or measurement locations to zero. Then, for levels $k \geq 2$, we compute $A_{6;\text{str}} = 4939$, $B_{6;\text{str}} = \frac{153}{3} = 5.8 \cdot 10^5$ and so $A_{6;\text{str}}^0 = 5054$. Thus, we obtain the recursion equations

$$\begin{aligned} {}^{(1)}_6 & 13;240 \cdot {}^{(1)}_6^2; \\ {}^{(k)}_6 & 5054 \cdot {}^{(k-1)}_6^2 \quad \text{for } k > 1; \end{aligned} \quad (16)$$

which imply the condition ${}^{(1)}_6 < 1.97 \cdot 10^{-4}$ or ${}^{(1)}_6 < 1.21 \cdot 10^{-4}$. Hence, $1.21 \cdot 10^{-4}$ is our accuracy threshold lower bound for adversarial stochastic noise.

For KnFTEC, the analogous coefficients ${}_{ij}$ of Eq. (13) are found to be

$$\begin{array}{ccccc} 0 & & 1 & & \\ \begin{array}{c} 60 \\ 60 \quad 30 \\ 60 \quad 0 \quad 30 \\ 180 \quad 0 \quad 180 \quad 270 \\ 180 \quad 180 \quad 0 \quad 0 \quad 270 \\ 1104 \quad 552 \quad 552 \quad 1656 \quad 1656 \quad 4164 \end{array} & & \begin{array}{c} C \\ C \\ C \\ C \\ C \\ A \end{array} & : & \end{array} \quad (17)$$

Taking all error rates to be equal, $A_6 = 11;184$ and we find $A_6^0 = 11;558$. This indicates a lower bound of $8.65 \cdot 10^{-5}$ on the accuracy threshold.

This bound can also be improved by "stretching." For levels $k \geq 2$, we compute $A_{6;\text{str}} = 5328$. Furthermore, because of our observation in Section C in this Appendix, we can take the transversal Bell measurements in the leading KnFTEC gadgets inside the cnot extended rectangle to be ideal. This reduces the effective number of locations in this extended rectangle from 297 to $297 - 27 = 243$ at level 1, and from 153 to $153 - 9 = 135$ at levels $k \geq 2$. The analogous recurrence equations give $1.26 \cdot 10^{-4}$ as our accuracy threshold lower bound using KnFTEC.

As discussed in the main text, a threshold analysis for depolarizing noise must take account of the fact that coding modulates the effective noise channel that acts at coding levels $k \geq 2$ by inducing effective correlations. However, we can establish a lower bound on the depolarizing threshold which exceeds our lower bound for adversarial stochastic noise by the following procedure: Considering the first coding level separately, we can find the critical error rate below which one level of coding improves the accuracy under depolarizing noise. Then, for all higher coding levels, we can use our bounds obtained for adversarial stochastic noise, since this will surely overestimate the effective correlations at these levels.

At the first coding level, a similar computer-aided combinatorial analysis is used to find the depolarizing noise coefficients [11], from which we determine $A_{6;\text{depol}} = 6969.89$ for SteFTEC and $A_{6;\text{depol}} = 5516.51$ for KnFTEC. Combining these results with our combinatorial coefficients for adversarial noise at coding levels $k \geq 2$, we find depolarizing noise threshold lower bounds of $1.60 \cdot 10^{-4}$ using SteFTEC and $1.76 \cdot 10^{-4}$ using KnFTEC.

The $[25,1,5]$ $C_{BS}^{(5)}$ code

$C_{BS}^{(5)}$ is a two error correcting code. Despite its large block size relative to its distance, our fault-tolerant quantum circuits are more compact and efficient relative to constructions for other interesting CSS codes of high distance as, e.g., the Golay [23,1,7]. In fact, Table I shows that the cnot extended rectangle for $C_{BS}^{(5)}$ contains 1,185 locations, when the corresponding extended rectangle for the Golay code contains 7,551 locations [Reichardt, Ouyang; unpublished].

The stabilizer group for $C_{BS}^{(5)}$ is generated by

$$\begin{aligned} S(C_{BS}^{(5)}) = & hX_{\text{row } i; \text{row } (i+1)}; \\ & Z_{\text{col } j; \text{col } (j+1)} \quad j; j+2 \leq Z_{4i}; \end{aligned} \quad (18)$$

FTEC using measurements on the gauge qubits can be implemented with the circuits shown in Fig. 21. In order to satisfy fault-tolerance properties 0, 1 in Ref. [11], we need to add some redundancy in our syndrome measurements. For example, syndrome extraction could be repeated.

For SteFTEC, we prepare five-qubit cat states as is, e.g., shown in Fig. 22. This time the cat states need verification to prevent a single fault from causing more than one X and/or Z error that will propagate to the subsequent transversal measurements. Alternatively, verification can be replaced by repeated syndrome extraction. These cat states can be used to collect the syndrome similarly to Fig. 20 for $C_{BS}^{(3)}$.

An analysis of malignant triples of faults gives for the joint probability of error for the level- k cnot extended

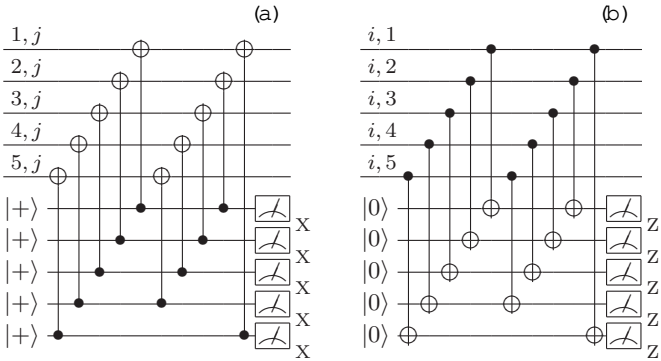


FIG. 21: FTEC for $C_B^{(5)}$ using m measurements on the gauge qubits. (a) Measuring operators in T along column n , j . (b) Measuring operators in T along row i . Identical circuits are run in parallel for all rows and columns $i, j \in \mathbb{Z}_5$. Some form of redundancy is necessary to ensure fault tolerance; e.g., the syndrome extraction could be repeated. A gain, all these m measurements could be executed sequentially using a single ancillary qubit.

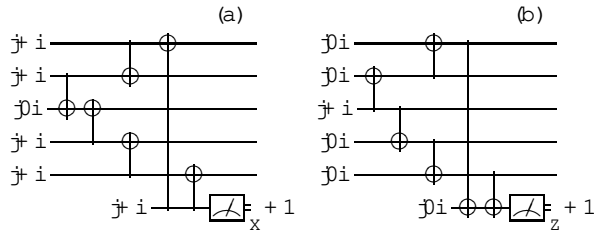


FIG. 22: (a) A 7-qubit cat state in the Hadamard-rotated basis with verification against Z errors. (b) A 7-qubit cat state with verification against X errors.

rectangle and a successful outcome in all of the verification tests:

$$\begin{matrix} (k) & X^6 \\ 6; \text{point} & ij, \begin{matrix} (k-1) \\ i \end{matrix} \begin{matrix} (k-1) \\ j \end{matrix}, \begin{matrix} (k-1) \\ m \end{matrix} + B \left(\begin{matrix} (k-1) \\ \max \end{matrix} \right)^4 : \\ & \begin{matrix} i \\ j \end{matrix} \begin{matrix} i=1 \end{matrix} \end{matrix} \quad (19)$$

As in Ref. [11], the probability of a successful outcome in a verification test is

$$P_{\text{accept}}^{(k)} \quad 1 \quad \underset{m \text{ ax}}{(k-1)} \quad C_6; \quad (20)$$

where C_6 is the total number of locations in the encoding and verification circuit for all cat states contained in one SteFTEC step. Taking all error rates to be equal, the error probability of the level- k CNOT extended rectangle conditioned on the successful outcome in all verification tests is

$$(k) \quad 1 \quad (k-1) \quad {}^{4C_6} (A_6 + B_6 (k-1)) (k-1)^3; \quad (21)$$

where $A_6 = 16,625,488$ is the total number of alignant triples, $B_6 = \frac{1185}{4}$, and $C_6 = 190$.

As we did for $C_{BS}^{(3)}$, for all concatenation levels $k \geq 2$, we can consider stretched extended rectangles. Then, for levels $k \geq 2$ we only keep the coefficients a_{ij} that do not involve preparation or measurement locations. Since $a_{111} = 287;460$, $a_{116} = 1;899;918$, $a_{166} = 3;911;460$, and $a_{666} = 2;554;190$, we have $A_{6,str} = 8;653;028$. From the error-correction circuits, we have $B_{6,str} = \frac{705}{4}$, and $C_{6,str} = 120$. Solving for the fixed point of our recursion equations, we obtain $1.94 \cdot 10^{-4}$ as our lower bound on the accuracy threshold.

Our calculations for the Monte-Carlo malignant-fault analysis are similar and will not be included here. Also, the circuit constructions and threshold analysis for $C_{BS}^{(7)}$ are similar to $C_{BS}^{(3)}$ and $C_{BS}^{(5)}$ and will be omitted.

[A 1] D . Poulin. Phys. Rev. Lett. 95, 230504 (2005).

[A 2] S. Bravyi and A . Yu. K itaev. arX ive e-print quant-ph/9811052.

[A 3] D . P.D i V incenzo and P . Shor. Phys. Rev. Lett. 77, 3260 (1996).

[A 4] E . D ennis, A . K itaev, A . Landahl, and J. P reskill. J. Math. Phys. 43, 4452 (2002).

[A 5] J. P reskill. Introduction to Quantum Computation, p. 213{269, eds. H .-K . Lo and S. Popescu and T . P . Spiller, W orld S cientific, Singapore (1998).

[A 6] D . P. D i V incenzo and P. A liferis. arX ive e-print quant-ph/0607047.

[A 7] D . G otteman. P roblem 4, set 5, C & O 639, U niversity of W aterloo, 2004. <http://www.perimeterinstitute.com/personal/dgottesman/C0639-2004/>

[A 8] J. P reskill. Ph/C S 219, Caltech, 2005. <http://www.theory.caltech.edu/people/preskill/ph229/>

[A 9] E . K nill. arX ive e-print quant-ph/0402171.

[A 10] S. Bravyi and A . Yu. K itaev. Phys. Rev. A 71, 022316 (2005).

[A 11] One X and one Z error in different data qubits is not, strictly speaking, acceptable since the resulting state has a weight-two error and will not pass through a 1- liter [11]. However, for the cnot, cphase and H adamard exRecs which determine the accuracy threshold (the logicalphase and To oligates can be implemented at the highest concatenation level as discussed in Section C), defining the 1-liter as treating X and Z errors separately is sufficient for fault-tolerance. This is because cnot and cphase do not mix X and Z errors upon conjugation and the H adamard transform s X errors to Z errors and vice versa.

[A 12] An error in the eigenvalue of $X_{1;j}X_{2;j}$ will lead us to incorrectly infer an error $Z_{1;j}$ in the data if we do not perform the extra measurement of $X_{1;j}X_{3;j}$. Combining $Z_{1;j}$ with $Z_{2;j}$ leads to an uncorrectable error in the data caused by a single faulty cnot.

[A 13] P. A liferis and B . M . Terhal. Quantum Inf. Comp. 7, 139{157 (2007).